Ultrafast Changes in the Optical Properties of a Titanium Surface and Femtosecond Laser Writing of One-Dimensional Quasi-Periodic Nanogratings of Its Relief

E. V. Golosov[a], A. A. Ionin[b], Yu. R. Kolobov[a], S. I. Kudryashov[b,*], A. E. Ligachev[c], Yu. N. Novoselov[b], L. V. Seleznev[b], and D. V. Sinitsyn[b]

[a] *Belgorod State University, Belgorod, 308015 Russa*

[b] *Lebedev Physics Institute, Russian Academy of Sciences, Moscow, 119991 Russia*

[c] *Prokhorov General Physics Institute, Russian Academy of Sciences, Moscow, 119991 Russia*

**e-mail: sikudr@sci.lebedev.ru*

Abstract—One-dimensional quasi-periodic nanogratings with spacings in the range from 160 to 600 nm are written on a dry or wet titanium surface exposed to linearly polarized femtosecond IR and UV laser pulses with different surface energy densities. The topological properties of the obtained surface nanostructures are studied by scanning electron microscopy. Despite the observation of many harmonics of the one-dimensional surface relief in its Fourier spectra, a weak decreasing dependence of the first-harmonic wavenumber (nanograting spacing) on the laser fluence is found. Studies of the instantaneous optical characteristics of the material during laser irradiation by measuring the reflection of laser pump pulses and their simulation based on the Drude model taking into account the dominant interband absorption allowed us to estimate the length of the excited surface electromagnetic (plasmon–polariton) wave for different excitation conditions. This wavelength is quantitatively consistent with the corresponding nanograting spacings of the first harmonic of the relief of the dry and wet titanium surfaces. It is shown that the dependence of the first-harmonic nanograting spacing on the laser fluence is determined by a change in the instantaneous optical characteristics of the material and the saturation of the interband absorption along with the increasing role of intraband transitions. Three new methods are proposed for writing separate subwave surface nanogratings or their sets by femtosecond laser pulses using the near-threshold nanostructuring, the forced adjustment of the optical characteristics of the material or selecting the spectral range of laser radiation, and also by selecting an adjacent dielectric.

1. INTRODUCTION

It was recently found that, by exposing the surfaces of solid materials to visible and near-IR femtosecond laser pulses, reproducible subwave (spacing $\Lambda = 70$–$900\ \text{nm} \leq \lambda$, where λ is the laser excitation wavelength) one-dimensional and two-dimensional quasi-periodic nanoscale structures (nanogratings) can be fabricated [1–8]. Such gratings on the surfaces of various materials are of interest because the nanoscale relief with elements from 1 to 100 nm in size imparts to the surface layer unusual physicochemical properties continuously changing depending on Λ [4] in the range from atomic/molecular to volume values for these materials. The relief periodicity gives to the surface interesting electronic and optical properties caused by a change in the spectrum of surface electromagnetic waves (SEWs or plasmon–polaritons) due to their partial localization [9, 10]. As a result, materials with surface nanogratings reveal superhydrophobic or superhydrophilic behavior [11, 12], the giant amplification of nonlinear optical processes in adsorbed atoms or molecules [10] and almost 100% absorption [13, 14] along with the absorption spectrum broadening [13]. Upon femtosecond laser writing of surface nanogratings in liquids, the surface relief often serves as a source of chemically pure nanoparticles [15, 16] accumulated as a sol, which can be used, for example, as nanoluminescent biomarkers [16].

The prospects for continuously changing the properties of one-dimensional surface nanogratings in a broad range by adjusting the grating spacing Λ by varying the laser radiation parameters and selecting proper writing materials has initiated a number of investigations. The value of Λ can obviously be varied by changing the laser radiation polarization (vector $\mathbf{e}$), the laser pulse wavelength and duration, the laser fluence F, and the number N of incident laser pulses [1–8]. In particular, it was found that wavevector $\mathbf{q}$ of nanogratings is in most case collinear to $\mathbf{e}$, while the grating spacing Λ linearly increases with increasing λ for ultrashort (femto- and short picosecond) laser pulses I a rather limited range covering the visible and near-IR

regions [6, 7]. The prolonged irradiation of a surface by short laser pulses usually makes it possible to develop only a nano- or microstructure produced initially on the surface. However, in the case of ultrashort laser pulses, the exposure time gives only additional possibilities for varying the type of interaction of laser radiation with matter (see, for example, [17]).

At first glance it would seem that, by varying parameters F [8] and N [7] within a few orders of magnitude, it is possible to change Λ quite efficiently. However, it has been shown in earlier papers that the value of Λ hardly changed at all with increasing exposure time (the number N of pulses), and only the development or degradation of the initially produced nanostructure was usually observed [7]. At the same time, a change in the laser fluence of femtosecond laser radiation had no effect on Λ for some materials [3, 4], whereas for other materials this effect was considerable (for example, the grating spacing doubled with increasing F near the ablation threshold [8]). Such a relation between Λ and F complicates the fabrication of one-dimensional gratings with minimal possible spacings (smaller than 100 nm) of interest for modern nanotechnologies, because the nanoscale transfer of matter drastically slows down at lower energy densities. Recently it was found that, on the contrary, the spacing of one-dimensional nanogratings on a titanium surface decreased with increasing energy density [18], which can be tentatively explained by a change in the instantaneous optical characteristics of titanium during excitation by an ultrashort laser pulse.

Note that simulation of the spacing of one-dimensional surface nanogratings by the "interference" method [19, 20] assuming interference of the electric fields of the incident and surface electromagnetic fields and the equality of the surface nanograting spacing Λ to the SEW length Λ_{SEW} for different materials irradiated by femtosecond laser pulses (by neglecting variations in the optical characteristics during the laser pulse or taking them into account) has so far not resulted in reasonable agreement between the calculated values of Λ_{SEW} and experimental values of Λ. This is evidently explained by the fact that the results of simulations of instantaneous optical characteristics of photoexcited materials are insufficiently reliable (without comparison with actual experimental characteristics) and the choice of the characteristic spacing of surface nanogratings from a variety of gratings observed in experiments, including high harmonics of the nanorelief, is complicated [21–23].

In this paper, we studied the instantaneous optical characteristics of a titanium surface by measuring the reflection of femtosecond IR-laser pulses. The saturation of interband absorption dominant in the unexcited material was found and the increase in the intensity of intraband transitions was observed with increasing incident radiation energy density. The calculated optical characteristics of excited titanium, which agree well with the experimental dependence of the reflection coefficient of exciting laser pulses, allowed us to estimate the lengths of SEWs excited on dry and wet titanium surfaces, which coincide with spacings of the first harmonic of the observed quasi-periodic surface nanorelief.

We selected titanium for investigations because it is one of the main construction materials for aircraft construction and ship building, as well as for medical bioimplants, so that the nanostructuring of its surface can impart new useful properties to it. In addition, as shown below in Section 3, being a transition metal, titanium has strong interband and considerable intraband absorption in the optical range, and therefore, similarly to semiconductors, its optical properties can change substantially (in the direction of metallization) upon intense excitation by femtosecond laser pulses. The latter effect is of interest for the femtosecond laser generation of one-dimensional periodic surface nanogratings with spacings varying in a broad range.

2. EXPERIMENTAL

We used an experimental setup consisting of an Avesta Project Ti:sapphire laser emitting 8-mJ, 110-fs first-harmonic pulses at $\lambda_{las1} \approx 744$ nm (the laser line FWHM was about 12 nm) and 0.5-mJ, 60-fs third-harmonic pulses at $\lambda_{las3} \approx 248$ nm (the FWHM ~ 1.5 nm) [24]. The transverse spatial distribution of the laser radiation intensity corresponded to the TEM_{00} mode in both cases. Normally incident laser radiation was focused into a spot 0.5 mm in diameter (at the $1/e$ level) on the surface of a target (a rod 8 mm in diameter) made of chemically pure multiply annealed and mechanically polished (rms $\leq$ 50 nm) BT1-0 titanium with the mean grain size of 0.25 μm (Center of Nanostructure Materials and Technologies, Belgorod State University) mounted horizontally on a three-axis motorized computer-controlled stage (Avesta Project) (Fig. 1).

The titanium target was irradiated by N laser pulses in air or an in plastic cell under a thin layer of distilled water 1–1.5 mm in thickness (only for IR radiation). The laser pulse energy was controlled by means of a reflective polarization attenuator (Avesta Project) and a calibrated DET-210 photodiode (Thorlab) illuminated by a weak laser pulse reflected from a steering dielectric mirror.

Nanostructured parts in the form of individual dots or strips were written, respectively, when the titanium target was in rest or by scanning its surface at a rate of 20 μm/s. The writing was performed by low-energy laser radiation (less than 0.3 mJ, peak power $W <$ 3 GW) to avoid noticeable distortion of the energy density distribution on the target surface caused by self-focusing in air (the critical self-focusing power was $W_{cr} \approx 3$ GW at a wavelength of 744 nm [25]) and

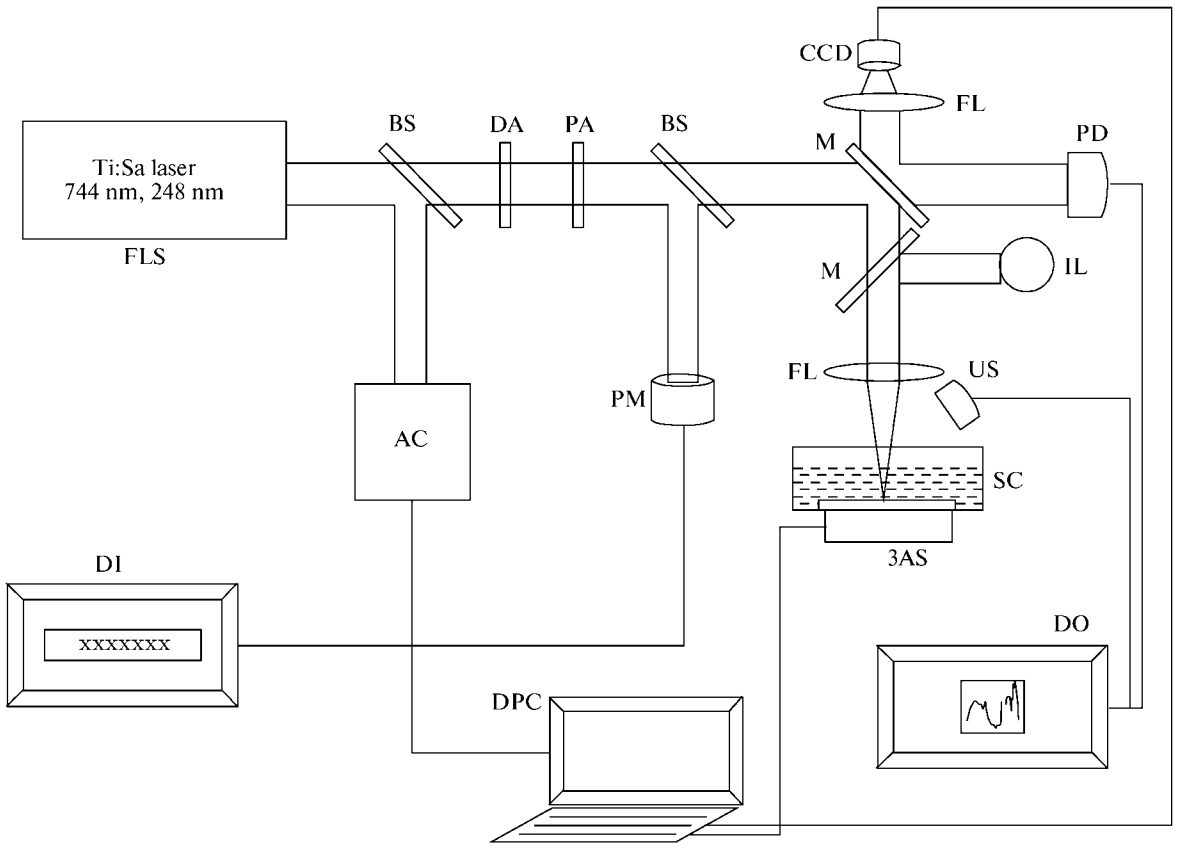

Fig. 1. Diagram of the experimental setup for nanostructure writing by femtosecond laser pulses: FLS: femtosecond laser system; BS: beamsplitter; AC: autocorrelator; DA and PA: diffraction and polarization attenuators; PM: pyroelectric power meter; M: mirror; FL: focusing lens; CCD: CCD array for surface visualization; PD: fast photodiode for oscilloscope triggering; IL: illumination lamp; SC: plastic sample cell; DO: digital oscilloscope; US: ultrasonic sensor; 3AS: 3-axis computer-controlled motorized stage; DPC: data processing computer; DI: digital indicator.

the accompanying effects of refraction in a plasma, chromatic emission, and filamentation [25, 26], as well as by melting and ablation of the target (the melting and ablation thresholds in the IR range are $F_{melt} \approx$ 50–60 mJ/cm^2 and $F_{abl} \approx 300$ mJ/cm^2 [27]).

The microscale structure of the target surface after irradiation was preliminarily studied with a Levenhuk BioView 630 optical microscope (1000× magnification) equipped with a CCD camera. The nanoscale relief was analyzed with a Quanta FEG 6000 scanning electron microscope with magnification up to 200000×.

The instantaneous optical characteristics (optical quality) of the excited titanium surface were probed directly during the laser pump pulse by means of two calibrated pyroelectric power meters measuring the reflection coefficients R of focused femtosecond IR-laser pulses at angles of about 20° (R_p, p polarization) and 45° (R_s and R_p, s and p polarizations) in the single-pulse regime for different incident energy densities F in "fresh" regions of the titanium surface.

3. EXPERIMENTAL RESULTS AND DISCUSSION

3.1. Self-Reflection of Femtosecond Pump Laser Pulses and Simulation of Instantaneous Optical Characteristics of Photoexcited Titanium

It is known that the general description of optical properties of titanium in the near IR, visible, and UV ranges is quite complicated [28]. This is caused primarily by the presence of d bands with a high density of states $g_d \approx 2$ eV^{-1}, both filled (0.5 eV below the Fermi level) and unfilled (0.1 eV above the Fermi level), near the Fermi level E_F (in the s band with the low density of states $g_s \approx 0.5$ eV^{-1} at the Fermi level [29]). As a result, the allowed interband $d \longrightarrow s^*$ transitions from the filled states of the d band below the Fermi level to the unfilled states of the s^* band lying higher can occur in the energy range $\hbar\omega > 0.3$ eV. The probability of these transitions greatly exceeds the probability of the interband $s \longrightarrow d^*$ transitions from the filled states of the s band below the Fermi level to the unfilled states of d^* band lying higher. Correspondingly, the contribution of intraband transitions (the Drude contribu-

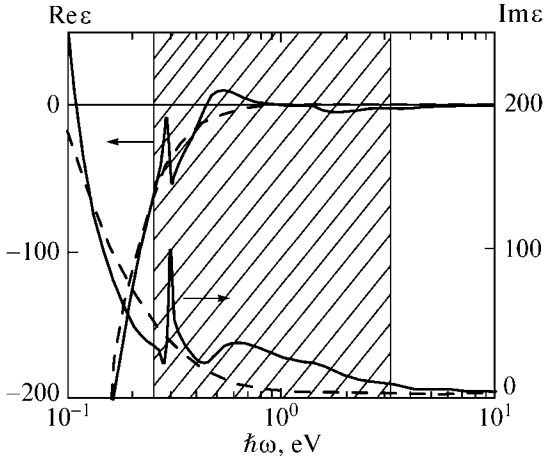

Fig. 2. Spectral dependences of the real and imaginary parts of the titanium permittivity [28] (dashed curves are approximations of these dependences using the Drude model). The interband transitions dominate in the hatched region.

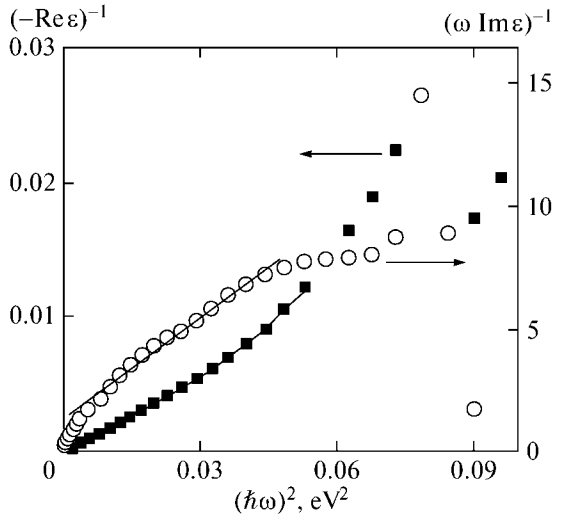

Fig. 3. Quadratic and linear approximations of dependences $(-\mathrm{Re}\varepsilon)^{-1}$ and $(\omega\,\mathrm{Im}\varepsilon)^{-1}$ on $\hbar\omega^2$ in the region $\hbar\omega$ = 0–03 eV, where interband absorption is negligible compared to intraband absorption [28].

tion) $\varepsilon_{\mathrm{intra}}$ to the permittivity ε of titanium proves to be considerably smaller than the contribution $\varepsilon_{\mathrm{inter}}$ of the interband transitions (Fig. 2). Thus, titanium behaves rather like a semiconductor. Therefore, one of the tasks of our work was to estimate these contributions in the energy region $\hbar\omega$ = 1–6 eV.

The contributions of intraband ($\varepsilon_{\mathrm{intra}}$) and interband ($\varepsilon_{\mathrm{inter}}$) transitions to the permittivity ε of titanium in the visible and UV ranges, including the corresponding parameters ω_{pl} and τ_{ee}, were determined by approximating the permittivity using the Drude model in the IR region ($\hbar\omega < 0.3$ eV), where absorption between the *d* and *s* bands is absent [28] (Fig. 2). Taking into account the expression

$$\tau_{ee} = K_{ee}^{-1}\frac{1+\exp[-\hbar\omega/k_{\mathrm{B}}T_e]}{(\pi k_{\mathrm{B}}T_e)^2+(\hbar\omega)^2}, \qquad K_{ee} = \frac{\pi^2\sqrt{3}\omega_{\mathrm{pl}}}{128E_{\mathrm{F}}^2}, \tag{1}$$

for the relaxation time τ_{ee} in the Fermi liquid [30], the general expressions for the Drude contributions $\mathrm{Re}\varepsilon_{\mathrm{intra}}$ and $\mathrm{Im}\varepsilon_{\mathrm{intra}}$ to the permittivity

$$\mathrm{Re}\varepsilon_{\mathrm{intra}} = -\frac{\omega_{\mathrm{pl}}^2\tau_{ee}^2}{1+\omega^2\tau_{ee}^2}, \qquad \mathrm{Im}\varepsilon_{\mathrm{intra}} = \frac{\omega_{\mathrm{pl}}^2\tau_{ee}}{\omega(1+\omega^2\tau_{ee}^2)}, \tag{2}$$

can be written for the "cold" Fermi liquid (the electron temperature $T_e \approx 0$) in the form of the second- and first-degree polynomials with a variable $x = (\hbar\omega)^2$ (Fig. 3):

$$-\frac{1}{\mathrm{Re}\varepsilon_{\mathrm{intra}}} = \frac{K_{ee}^2}{\omega_{\mathrm{pl}}^2}(\hbar\omega)^4 + \frac{1}{(\hbar\omega_{\mathrm{pl}})^2}(\hbar\omega)^2, \qquad \frac{1}{\omega\,\mathrm{Im}\varepsilon_{\mathrm{intra}}} = \frac{K_{ee}}{\omega_{\mathrm{pl}}^2}(\hbar\omega)^2 + \frac{1}{K_{ee}(\hbar\omega_{\mathrm{pl}})^2}. \tag{3}$$

This allowed us to directly determine the plasma frequency $\omega_{\mathrm{pl}} = 3.9 \times 10^{15}$ rad/s and the electron–electron scattering constant $K_{ee} = 4.5 \times 10^{15}$ eV^{-2} s^{-1} for the unexcited material. The values of $\mathrm{Re}\varepsilon_{\mathrm{intra}}$ and $\mathrm{Im}\varepsilon_{\mathrm{intra}}$ calculated by using these parameters were subtracted from the total permittivity ε (Fig. 2) and the interband components $\mathrm{Re}\varepsilon_{\mathrm{inter}}$ and $\mathrm{Im}\varepsilon_{\mathrm{inter}}$ were calculated in the range $\hbar\omega$ = 1–6 eV.

Irradiation by intense femtosecond laser pulses induces interband transitions from the *d* band with the high density of states to the *s* band with the low density of states, resulting in the population of the latter. This leads, on the one hand, to the interband absorption saturation and on the other hand to the increase in the number of carriers in the *s* band and in the plasma frequency ω_{pl}, while the relaxation time τ_{ee} decreases. As a result, the role of intraband transitions drastically increases at the expense of interband transitions. The influence of photoexcitation on ε is taken into account by using normalizing coefficients of the type $1 - N/N_{\mathrm{inter}}$ and $1 + N/N_{\mathrm{intra}}$ describing the interband absorption saturation ($N \le N_{\mathrm{inter}}$) and the increase in the density N of free carriers in the *s* band ($N > N_{\mathrm{intra}}$), respectively. The components $\varepsilon_{\mathrm{inter}}$ and $\varepsilon_{\mathrm{intra}}$ were multiplied by these factors, respectively. Taking into account the interband absorption saturation, the density of photo-

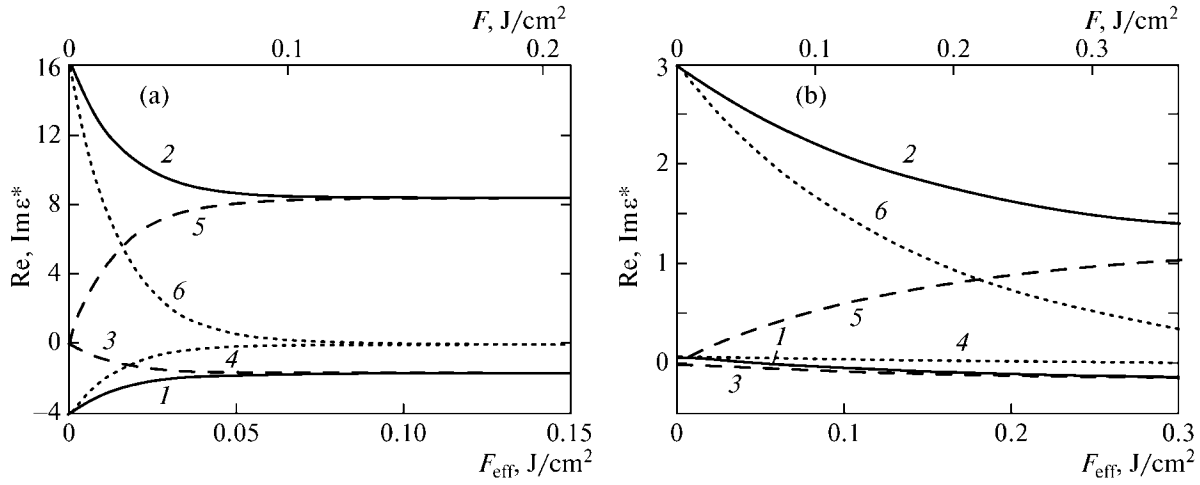

Fig. 4. Real (curves *1*) and imaginary (curves *2*) parts of the excited titanium permittivity ε^* for $\lambda_{las1} = 744$ nm (a) and $\lambda_{las3} = 248$ nm (b) with contributions $\mathrm{Re}\varepsilon_{intra}$ (curves *3*) and $\mathrm{Re}\varepsilon_{inter}$ (curves *4*) and positive contributions $\mathrm{Im}\varepsilon_{intra}$ (curves *5*) and $\mathrm{Im}\varepsilon_{inter}$ (curves *6*) as functions of the energy density.

excited carriers in the *s* band as a function of the effective (absorbed) energy density $F_{eff} = [1 - R(F)]F$ was calculated from the kinetic equation

$$\frac{dN}{dt} = \left(\alpha_0 \frac{N_{inter} - N}{N_{inter}}\right) \frac{I_{eff}}{\hbar\omega} \tag{4}$$

with the solution

$$N(F_{eff}) = N_{inter}\left[1 - \exp\left(-\frac{\alpha_0 F_{eff}}{N_{inter}\hbar\omega}\right)\right], \tag{5}$$

where α_0 is the absorption coefficient of the unexcited material at the laser excitation wavelength, the factor $\alpha_0(1 - N/N_{inter})$ is the effective absorption coefficient, and the integral of the effective radiation intensity I_{eff} during the laser pulse is F_{eff}. The calibration constant N_{inter} (wavelength-dependent in the general case) was found in the form of integrals from the g_d and g_s components of the electronic density of states [29]

$$\begin{aligned} N_{inter} &= \frac{N_A}{V_M}\int_{-E_d}^{-E_{ds}} g_d(E)dE \approx g_d(-E_{ds})\Delta_d \\ &= \frac{N_A}{V_M}\int_0^{E_s} g_s(E)dE \approx g_s(0)\Delta_s, \end{aligned} \tag{6}$$

where $N_A \approx 6 \times 10^{23}$ mol^{-1} is the Avogadro constant, $V_M \approx 10.5$ cm^3/mol is the molar volume of the titanium phase with hexagonal packing, $-E_d$ is the energy level in the *d* band below the Fermi level (the Fermi level energy *E* is set equal to zero), $-E_{ds}$ is the top of the *d* band with respect to the Fermi level, E_s is the energy level in the *s* band above the Fermi level, and the integration intervals $\Delta_d = -E_d - (-E_{ds})$ and $\Delta_s = E_s$ were determined by the expression

$$\Delta_d + E_{ds} + \Delta_s = \hbar\omega. \tag{7}$$

As a result, for $g_s(0) \approx 0.5$ eV^{-1}, $g_d(-E_d) \approx 2$ eV^{-1}, $\Delta_s \approx 0.7$ eV, and $\Delta_d \approx 0.3$ eV, the value of N_{inter} for radiation at $\lambda = 774$ nm was 3.6×10^{22} cm^{-3} (1.3×10^{23} cm^{-3} at $\lambda = 248$ nm). In turn, the calibration constant N_{intra} related to the initial density of free carriers in the *s* band for the unexcited titanium was estimated based on its plasma frequency $\omega_{pl} = 3.9 \times 10^{15}$ rad/s, which gave the effective density of carriers $N_s/m_s \approx 4 \times 10^{21}$ cm^{-3}, where m_s is the unknown mass of carriers in the *s* band. Note that the best fit of experimental data was achieved for $N_{intra} \approx 2 \times 10^{21}$ cm^{-3}, which corresponds to $m_s \approx 0.5$.

As a result, the permittivity ε^* of the photoexcited titanium was considered in the form

$$\begin{aligned} \mathrm{Re}\varepsilon^* &= \mathrm{Re}\varepsilon_{inter}\left(1 - \frac{N}{N_{inter}}\right) \\ &+ \mathrm{Re}\varepsilon_{intra}\left(1 + \frac{N}{N_{intra}}\right), \\ \mathrm{Im}\varepsilon^* &= \mathrm{Im}\varepsilon_{inter}\left(1 - \frac{N}{N_{inter}}\right) \\ &+ \mathrm{Im}\varepsilon_{intra}\left(1 + \frac{N}{N_{intra}}\right). \end{aligned} \tag{8}$$

Note that the temperature of the Fermi liquid was assumed much lower than the laser photon energy $\hbar\omega(774\ \mathrm{nm}) = 1.7$ eV because a narrow dielectric gap between the *d* and *s* bands (more exactly, between the

Fermi level and the latter) $E_{ds} \approx 0.3$ eV [28, 29] restricts the temperature rise due to impact ionization at the level on the order of E_{ds}. Therefore, the influence of the electron temperature T_e on the relaxation time τ_{ee} of carriers until the complete saturation of interband absorption ($N \le N_{inter}$) was neglected.

Our calculations show that for $\lambda_{las1} = 744$ nm, the interband absorption ($\alpha_0 = 6.6 \times 10^5$ cm^{-1} for the unexcited titanium [28]) disappears for $F_{eff} \ge 0.05$ J/cm^2 ($F \ge 0.09$ J/cm^2) together with the corresponding contributions to ε^* from $\mathrm{Re}\,\varepsilon_{inter}$ and $\mathrm{Im}\,\varepsilon_{inter}$ (Fig. 4a), whereas the intraband absorption increases together with $-\mathrm{Re}\,\varepsilon_{intra}$ and $\mathrm{Im}\,\varepsilon_{intra}$, saturating above the indicated threshold. On the contrary, for $\lambda_{las3} = 248$ nm, the interband absorption ($\alpha_0 = 7.3 \times 10^5$ cm^{-1} for the unexcited titanium [28]) disappears only for $F_{eff} > 0.3$ J/cm^2 together with the corresponding contributions $\mathrm{Re}\,\varepsilon_{inter}$ and $\mathrm{Im}\,\varepsilon_{inter}$ into ε^* (Fig. 4b). However, although contributions $-\mathrm{Re}\,\varepsilon_{intra}$ and $\mathrm{Im}\,\varepsilon_{intra}$ related to intraband transitions increase by many times in this case (by $N_{inter}/N_{intra} \approx 60$ times for $N_{inter} \approx 1.3 \times 10^{23}$ cm^{-3} and $N_{intra} \approx 2 \times 10^{21}$ cm^{-3}), their absolute value proves to be insufficient even for excitation of surface plasmons ($\mathrm{Re}\,\varepsilon^*$, $\mathrm{Re}\,\varepsilon_{intra} > -1$).

The dependence $R_p(20°, F)$, the reflection coefficient of pump pulses, on the energy density for $\lambda_{las1} = 744$ nm monotonically decreases (Fig. 5), which is typical not only for titanium with its dominating interband absorption in the optical range, but also for other metals, in particular, metals with the dominating Drude response (intraband absorption) [31]. For comparison, similar dependences of the reflection coefficients $R_{p,s}(45°, F)$ of pump pulses on the energy density in the initial region also monotonically decrease (inset in Fig. 5). At the same time, simulation of the optical properties of photoexcited titanium and, in particular, calculated curves $R_p(20°, F)$ and $R_{p,s}(45°, F)$ (Fig. 5) show that the initial decrease in the reflection coefficient of titanium with its increasing photoexcitation level is explained by the saturation of interband absorption in titanium, whereas the subsequent decrease can be related to the heating of the Fermi liquid [31].

The optical characteristics estimated for photoexcited titanium were used below to calculate the dependence of the SEW length excited on its surface by femtosecond laser pulses at 744 and 248 nm and to specify, according to the interference model, the period of the fundamental harmonic of its surface relief on laser energy density F.

3.2. Production of One-Dimensional Quasi-Periodic Nanogratings of a Titanium Surface Relief in Air and Water

3.2.1. Writing of one-dimensional nanogratings in air. In the writing of nanostructures on the titanium target surface using a scanning electron microscope at

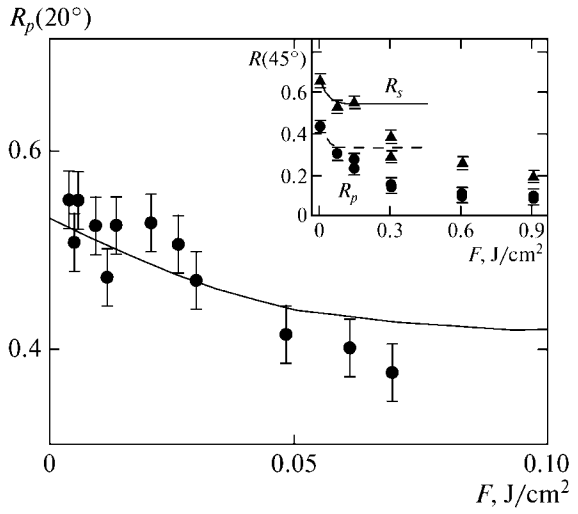

Fig. 5. Experimental (points) and calculated (curves) dependences $R_p(20°, F)$ for $\lambda_{las1} = 744$ nm. Inset: Dependences $R_{s,p}(45°, F)$ for the s (triangles, solid curve) and p polarizations (circles, dashed curve) of IR laser radiation.

low energy densities $F \approx 0.01$–0.15 J/cm^2 and a number of incident 744-nm laser pulses $N \approx 700$, we observed the formation of distinct one-dimensional gratings oriented perpendicular to the polarization of laser radiation ($\mathbf{q} \parallel \mathbf{v}, \mathbf{e}$) with spacings in the interval from 0.1 to 0.6 μm (Fig. 6). The lower boundary of the range of F values is approximately equal to the threshold $F_{NS,IR} \approx 0.018$ J/cm^2 of the production of such grooves for $N \approx 700$, because near this threshold the gratings have the form of quasi-periodic (with a mean spacing $\Lambda \approx 0.5$–0.6 μm) narrow (with a width $\Delta \le 0.1$ μm) grooves, which appear irregularly on the titanium surface, even taking into account fluctuations of the radiation energy within 5% (Fig. 6a). The target surface itself outside grooves does not contain any traces of its own material removal, but is contaminated by the fragments of ablation products reprecipitated from grooves (Fig. 6b). When the threshold $F_{NS,IR}$ is excited, surface nanogratings develop (cf. Figs. 6a and 6b); however, above an optimal value of F ($F \approx 0.03$ J/cm^3 for $N \approx 700$ in our case) (Fig. 6b), the grooves of the surface nanograting gradually degrade (Fig. 6c), for example, due to their noticeable melting (Fig. 6d).

Note that gratings with small spacings (0.1–0.3 μm) are present on the surface mainly near the nanostructuring threshold ($F \ge F_{NS,IR}$), where the relief grooves are nonsinusoidal (Fig. 6a). However, such gratings disappear almost completely for larger values of F (Figs. 6c, 6d), which is manifested in the amplitude spectra $S(q)$ of the fast Fourier transform in the form of the lower (mainly the second) harmonics of the nanorelief (Fig. 7) with a period multiple of the first-harmonic period $\Lambda_1 = 1/q_1$. Such a behavior can be explained by the diffraction of incident laser radia-

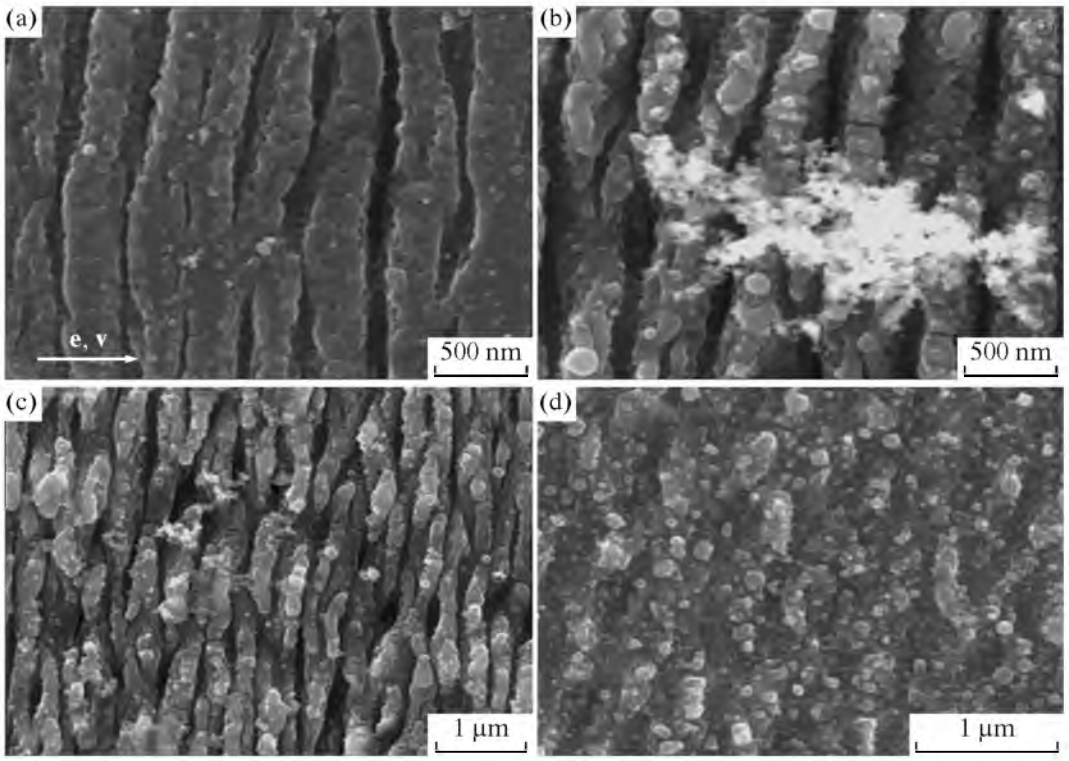

Fig. 6. Scanning electron microscope photographs of the titanium surface irradiated in air by IR 744-nm laser pulses for $N \approx 700$ and the energy density $F \approx 18$ (a), 27 (b), 36 (c), and 150 (d) mJ/cm^2. The arrows show the direction of polarization **e** and the sample scan rate **v**.

tion from the appearance of grooves of the intermediate nanorelief, according to the interference model [19, 20], due to interference of this radiation with an SEW (with the wavelength Λ_{SEW}) excited on the initially flat target surface. In this case, the distribution of the total energy density F_Σ of the electromagnetic field on the target surface has a periodic form along the direction of laser polarization (coordinate x) [32]:

$$F_\Sigma(x) = F(x) + \sqrt{FF_{SEW}}\sin\left(\frac{2\pi}{\Lambda_{SEW}}x + \phi\right), \qquad (9)$$

where F and F_{SEW} are the surface energy densities of the incident laser radiation and SEW, respectively, and ϕ is the initial phase. If the value of F_Σ at the interference maxima exceeds the nanostructuring threshold $F_{NS,IR}$ only slightly, then periodic shallow and narrow (width $\Delta \ll \Lambda_1, \Lambda_{SEW}$) grooves are produced (Fig. 8a), whereas for $F_\Sigma \gg F_{NS,IR}$ (but below the melting and ablation thresholds), the intermediate nanorelief $\xi(x)$ can have a quasi-harmonic character with period Λ_1 (Fig. 8b). It is important that in the latter case, for the quasi-harmonic reflecting surface grating (Fig. 8b) with a simple Fourier spectrum of the relief (Fig. 8d), the phase matching condition for diffraction of incident laser radiation has a simple form [33],

$$\mathbf{k}_t + n\mathbf{q}_g = \mathbf{k}_\parallel, \qquad (10)$$

where $\mathbf{k}_t$ and $\mathbf{q}_g$ are the projections of wavevectors of incident radiation $\mathbf{k}_0$ ($|\mathbf{k}_t| = |\mathbf{k}_0|\sin\theta$) and the surface grating on the target surface, θ is the angle between these projections, $\mathbf{k}_\parallel$ is the wavevector of the SEW, and the angular diffraction spectrum in each order n is represented by one component. On the contrary, in the first case, for the weakly modulated nonsinusoidal surface grating (Fig. 8a), the diffraction of laser radiation will occur from all harmonic gratings with frequencies in the Fourier spectrum of its profile (Fig. 8c). For this reason, the angular diffraction spectrum will contain a number of corresponding components. It is known that the amplitudes of angular components are proportional both to the amplitude (strength) of the incident laser wave and the amplitude ξ_q of the corresponding surface grating [20]. The angular components can propagate in a certain diffraction order along the surface and transform upon interference, according to (7), to surface nanogratings with spacings $\Lambda_m = \Lambda_1/m \ll \Lambda_1$ (m is the harmonic order) [34].

Thus, the production of a multiple spectrum of nanogratings on the surface of a material irradiated under certain conditions is most likely not caused by

the generation of the higher optical harmonics of optical radiation on the material surface, as was assumed in [21–23], but only characterizes the relation between the effective energy density F_Σ and the nanostructuring threshold $F_{NS,IR}$. Obviously, the primary characteristic of the SEW excited on the initially flat target surface and of preceding material photoexcitation processes and the subsequent development of the surface nanorelief is the fundamental (first) spatial harmonic of the nanorelief (Figs. 7 and 8) corresponding to the spacing Λ_1, but not a surface nanograting with a minimal spacing on the order of $\Lambda_m = \Lambda_1/m$ [8].

For different nanostructuring conditions for the titanium surface, primarily for different energy densities F, using the Fourier spectra on the surface nanorelief (including data in Fig. 7), we selected the wavelengths of the first harmonic of the nanorelief represented by the dependence $\Lambda_1(F)$ in Fig. 9. The period Λ_1 monotonically decreases with increasing F, like in [18], however, to a lesser degree. This discrepancy is probably explained by the better accuracy of the nanograting spacing analysis using the fast Fourier transform and by selecting the values of Λ_1 rather than the periods of higher harmonics, as in [18].

We recorded one-dimensional nanogratings on the titanium surface by femtosecond UV pulses ($\lambda_{las3} \approx$ 248 nm) with the energy density $F \approx 0.025$–0.1 J/cm^2. The number of incident pulses was $N \approx 10^2$, 3×10^2, and 10^3 (Figs. 10a, 10b). Similarly to nanogratings written by femtosecond IR pulses, the produced nanogratings were also oriented perpendicular to the polarization of laser radiation ($\mathbf{q} \parallel \mathbf{v}, \mathbf{e}$) and had subwave spacings in the range from 0.1 to 0.2 μm (Figs. 10a, 10b) and, as rule, the first and second relief harmonics with $\Lambda_1 \approx 0.18$–0.2 μm (Figs. 10c, 10d). The nanostructuring threshold for $N \approx 10^3$ femtosecond UV pulses was $F_{NS,UV} \approx 0.025$ J/cm^2, and the value of Λ_1 was virtually independent of F (Fig. 9).

3.2.2. Writing of one-dimensional nanogratings in water. Upon exposing a titanium target surface in water to $N \approx 10^4$ moderate-energy IR laser pulses ($F \sim$ up to 0.2 J/cm^2), we observed, instead of the titanium melting, the surface nanostructuring with the formation of regular one-dimensional gratings with $\mathbf{q} \parallel \mathbf{v}, \mathbf{e}$ and the minimal spacing $\Lambda \approx 0.09$–0.11 μm (Fig. 11a). In this case, similar gratings with $\Lambda \approx 0.1$ μm are produced at the laser spot periphery for F $\approx$ 0.1 J/cm^2. However, the irregular microscale modulation of the surface is also present in the form of curved and circular craters (Fig. 11b). The maximal spacing of one-dimensional nanogratings in both cases was $\Lambda_1 \approx 0.18$–0.2 μm (Figs. 11c, 11d).

The observation of unusual circular craters on the irradiated wet titanium surface for $F \approx 0.1$ J/cm^2 is probably a rather common manifestation of long-lived vapor/gas microbubbles [35] stabilized by the nanorough titanium surface. It is easy to show that for the given value of F, the conditions for water boiling on a considerable part of the irradiated surface are known

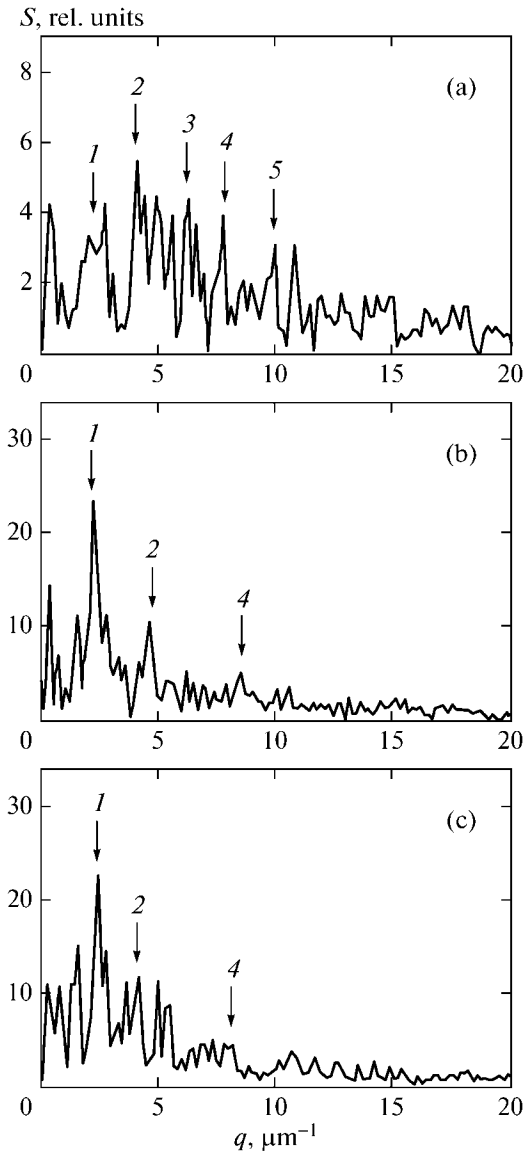

Fig. 7. Amplitude spectra of the fast Fourier transform for the surface nanorelief presented in Figs. 6a–6c. The arrows with numbers show the position of the corresponding harmonics of the nanorelief.

to be satisfied (the threshold and melting point for titanium are 0.05 J/cm^2 [27] and 1608°C [36], respectively, while the critical temperature T_{crit} of water is only 374°C [36]). The external walls of microbubbles are a natural waveguide with a large jump in the refractive index $\Delta n \approx 0.3$ [30], while the microbubbles themselves form a negative lens redistributing the incident laser radiation to the bubble periphery. This effect explains the appearance of narrow circular ablation craters on the titanium surface in water at such low mean energy densities $F \approx 0.1$ J/cm^2, which are evidently insufficient for direct ablation of the titanium surface (recall that the macroscopic ablation threshold

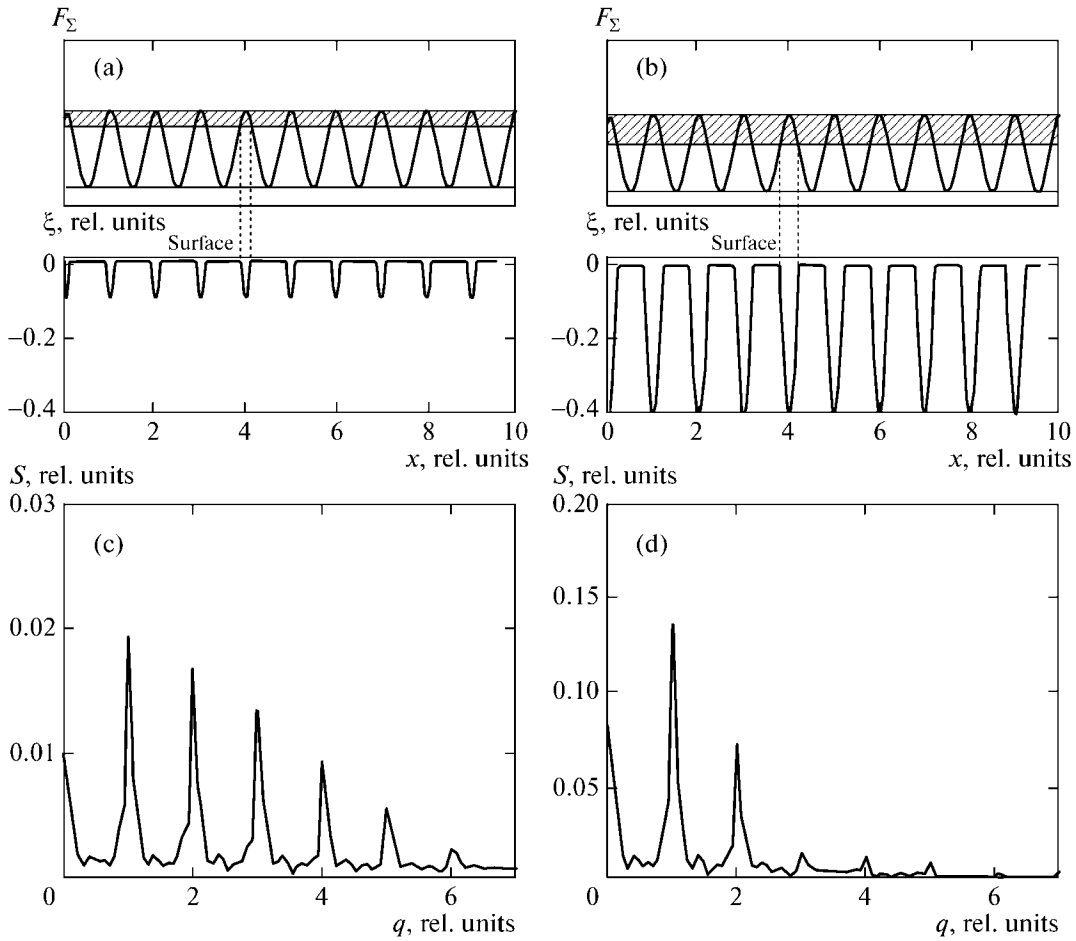

Fig. 8. (a, b) Model surface nanogratings represented by sinusoidal profiles truncated at levels 10% (a) and 40% (b) (the truncation level corresponds to the surface position). The upper sinusoids in both figures show the distribution of the total laser fluence F_Σ, and their parts in the hatched region are subjected to the surface material ablation (the value of F_Σ exceeds the ablation threshold). (c, d) Amplitude Fourier spectra of the surface nanorelief presented in Figs. 8a and 8b, respectively (integer lengths of the wavevector **q** represent the orders of the corresponding relief harmonics).

for titanium under our conditions is about 0.3 J/cm^2 [27]).

3.2.3. Simulation of basic spacings of one-dimensional nanogratings of the titanium surface relief. The spacings of one-dimensional gratings produced on the titanium surface by femtosecond IR and UV laser pulses were simulated using the interference model [19, 20] assuming that the basic spacing Λ_1 of such gratings is equal to the length Λ_{SEW} of an SEW excited on the initially flat target surface. In particular, when a SEW is generated that interferes with a light wave with the wavelength λ incident on a metal–dielectric interface, the Fourier component of the roughness with the wavevector $\mathbf{q} \parallel \mathbf{e}$ and period [33, 37]

$$\Lambda_{SEW} = \lambda\left(\sqrt{\frac{\mathrm{Re}\varepsilon_M \mathrm{Re}\varepsilon_D}{\mathrm{Re}\varepsilon_M + \mathrm{Re}\varepsilon_D}} \pm \sin\theta_{inc}\right)^{-1}, \qquad (11)$$

increases, where ε_M and ε_D are the permittivities of the metal and dielectric at the wavelength λ and θ_{inc} is the angle of incidence of radiation on the surface. Additional conditions of the SEW excitation have the form [37]

$$\mathrm{Re}\varepsilon_M + \mathrm{Re}\varepsilon_D < 0, \quad \mathrm{Re}\varepsilon_M \mathrm{Re}\varepsilon_D < 0. \qquad (12)$$

It was show earlier [18] that the estimates of periods Λ_1 from (11) based on the optical parameters of the unexcited material were in poor agreement with experimental data and did not allow determining the optimal conditions for femtosecond laser nanostructuring in the $\{\lambda, F, N\}$ space. Therefore, in this paper we made such estimates by using calculated instantaneous (during the exciting femtosecond laser pulse) optical characteristics of the photoexcited titanium (Fig. 4) that were in good agreement with experimental data (Fig. 5).

As a result, studies of titanium nanostructuring by femtosecond 744-nm laser pulses showed quantitative agreement between experimental values of Λ_1 and calculated values of Λ_{SEW} in the range F = 0.03–

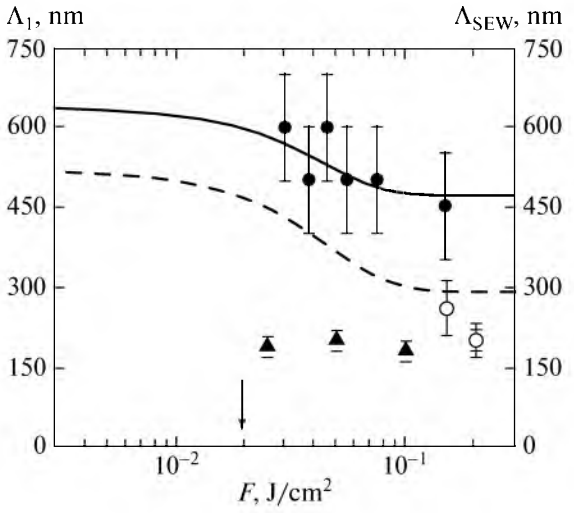

Fig. 9. Period Λ_1 of the first harmonic of the nanorelief as a function of the energy density F for $\lambda_{las1} = 744$ nm (in air: dark circles, in water: open circles) and $\lambda_{las3} = 248$ nm (in air: triangles). The solid and dashed curves are the model dependences of the SEW length Λ_{SEW} on F for dry and wet titanium surfaces, respectively, for $\lambda_{las1} = 744$ m.

$0.15\ \text{J/cm}^2 > F_{NS,IR}$ (Fig. 9). In accordance with results obtained in [1–8, 32, 38], the basic spacings of nanogratings produced in air ($\text{Re}\varepsilon_D \approx 1$) were weakly subwave (450–600 nm < 744 nm), according to expression (11) adapted to the case $\text{Re}\varepsilon_M \gg \text{Re}\varepsilon_D$

$$\frac{\Lambda_{SEW}}{\lambda} = \frac{1}{\sqrt{\text{Re}\varepsilon_D}}\left(1 - 2\left|\frac{\text{Re}\varepsilon_D}{\text{Re}\varepsilon_M}\right|\right). \qquad (13)$$

As result, the use of subwave nanogratings as one of the boundary dielectric media with high ε_D is promising. Indeed, for the same conditions of titanium nanostructuring in water ($\text{Re}\varepsilon_D \approx 1.75$ [36]) by femtosecond IR laser pulses, both calculated Λ_{SEW} and experimental spacings Λ_1 prove to be considerable smaller than $\lambda_{las1} = 774$ nm (Fig. 9).

The exposure of the titanium surface in air to 248-nm femtosecond laser pulses also leads to the production of small-scale one-dimensional nanogratings with subwave spacings from 0.1 to 0.2 μm, which is qualitatively explained, taking (11) and (13) into account, by a smaller laser radiation wavelength. At the same time, the simulation of SEW parameters in

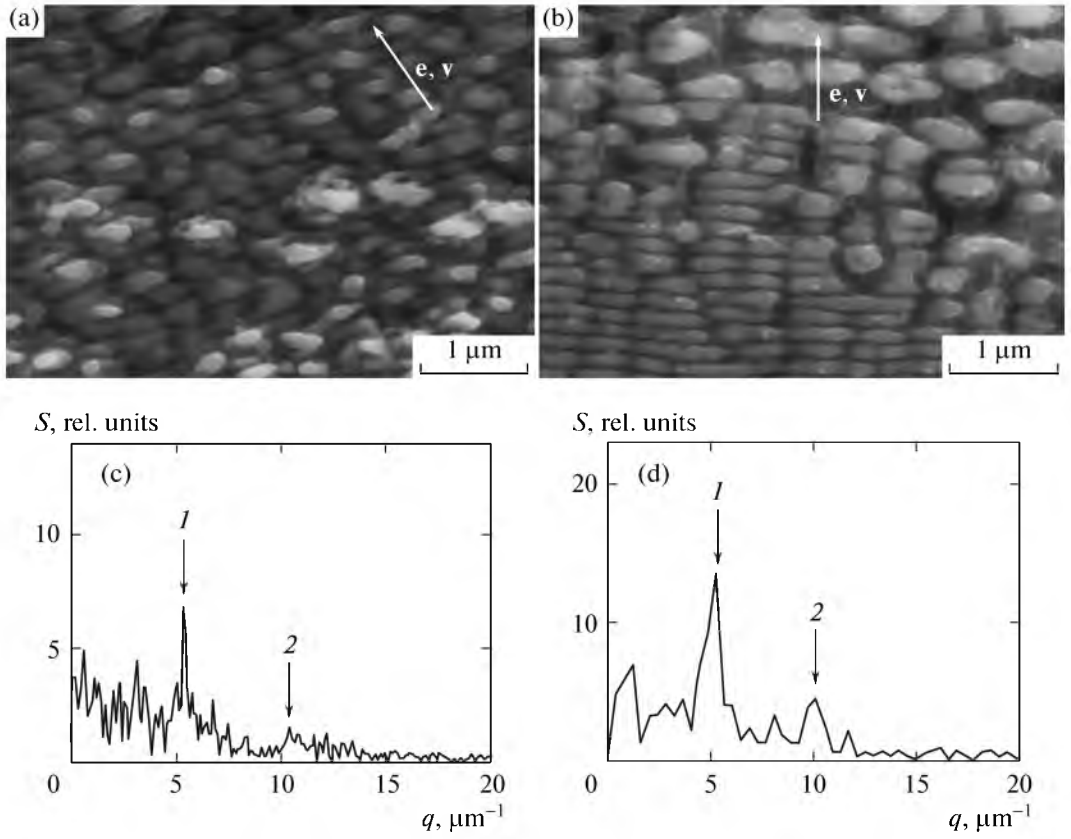

Fig. 10. Photographs of the titanium surface irradiated in air by 248-nm laser pulses for $N \approx 10^3$ and $F \approx 0.05\ \text{J/cm}^2$ (a) and $0.1\ \text{J/cm}^2$ (b). The arrows show the directions of polarization **e** and the sample scan rate **v**. (c, d) Amplitude Fourier spectra of the surface nanorelief presented in photographs above. The arrows with numbers show the position of the corresponding relief harmonics.

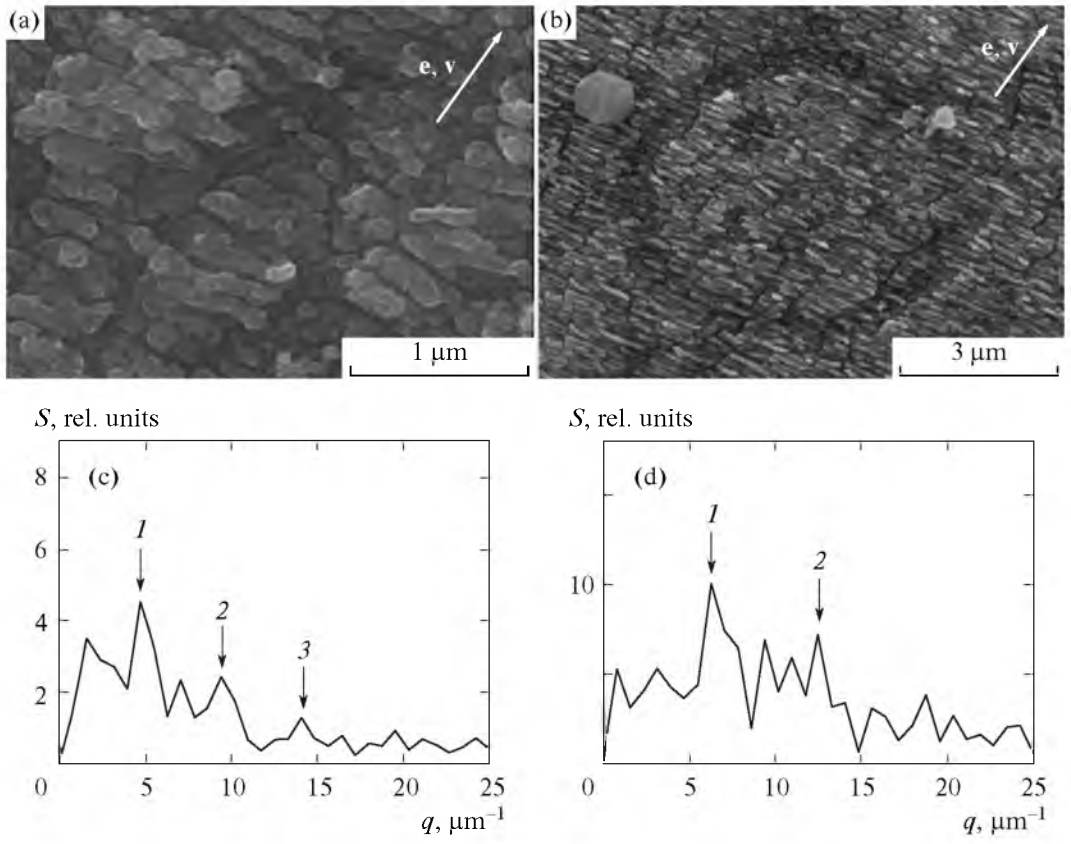

Fig. 11. Photographs of the titanium surface irradiated in water by 744-nm IR laser pulses for $N \approx 10^4$ and $F \approx 0.2$ J/cm^2 (a) and 0.1 J/cm^2 (b). The arrows show the directions of polarization **e** and the sample scan rate **v**. (c, d) Amplitude Fourier spectra of the surface nanorelief presented in photographs above. The arrows with numbers show the position of the corresponding relief harmonics.

the UV region proves rather complicated, because the Drude approximation with a constant initial plasma frequency and wavelength-dependent initial electron–electron scattering time of carriers (expressions (1) and (2)) in the mid-IR region (3–30 μm) (Fig. 3) is less accurate after its extrapolation to a broader spectral region including the UV range (Fig. 2). In particular, in this case it is necessary to take into account the unknown dispersion of the *s*-electron mass, which is probably quite considerable on passing from the mid-IR region to the UV region, which affects the initial value of the plasma frequency. As a result, for the Drude approximation of the titanium permittivity used here, the calculated value of $\mathrm{Re}\varepsilon_{\mathrm{intra}} < -1$ extrapolated from the mid-IR region to the UV region proves to be insufficient even for excitation of a SEW according to conditions (12).

4. CONCLUSIONS

We have studied the features of the quasi-periodic nanorelief written on a dry or wet titanium surface by femtosecond IR and UV laser pulses. It is assumed that oriented quasi-periodic structures (one-dimensional gratings) with subwave spacings are harmonics of the surface nanorelief produced due to the diffraction of incident laser pulses from an intermediate nonharmonic periodic surface grating. This intermediate surface nanograting is produced by the first laser pulses due to their interference by an SEW excited by them on a flat titanium surface and its subsequent ablation in spatial regions corresponding to the interference maxima. As a result, the spacing of the intermediate grating is equal, on the one hand, to the SEW length and, on the other hand, to the wavelength of the fundamental (first) harmonic of the nanorelief, which serves as a control parameter characterizing the SEW and its excitation conditions during a femtosecond laser pulse.

To understand the SEW excitation conditions on the titanium surface and the surface nanostructuring process, we simulated the instantaneous optical characteristics of photoexcited titanium using the model taking into account the bottleneck effect in the density of electronic states below and above the Fermi level for the *s* and *d* bands. Model calculations and the measured reflection coefficients of exciting femtosecond IR laser pulses showed that titanium, which is a semiconductor at optical frequencies, transforms to a conductor during ultrafast photoexcitation due to satura-

tion of the interband d–s absorption and the corresponding increase in the density of free carriers in the s band. As a result, the SEW length considerably changes. The SEW lengths calculated upon excitation of SEWs by femtosecond IR and UV laser pulses with different energy densities on the dry or wet titanium surfaces well agree with the periods of the first harmonics of the surface nanorelief.

We have proposed and considered three new methods for producing subwave quasi-periodic surface nanogratings by femtosecond laser pulses: (i) near (slightly above) the threshold nanostructuring energy density; (ii) in the region of the radiation energy density or radiation wavelength where the modulus of the real part of the permittivity of a photoexcited (conducting) medium approaches that for the permittivity of the adjacent dielectric ("laser field" and spectral tunings), and (iii) by the choice of the adjacent dielectric with the real part of the permittivity providing the condition indicated in (ii). These methods were not explicitly distinguished earlier probably because the physical nature of their basic processes was insufficiently clear. Note that these three methods in their entirety can be used to produce individual surface nanogratings or sets of them by laser pulses at different wavelengths with energy densities varying in a broad range.

ACKNOWLEDGMENTS

The authors thank G.A. Shafeev (General Physics Institute, RAS) for useful advice. This work was partially supported by the Russian Foundation for Basic Research (project nos. 08-08-00756-a, 09-02-12018-ofi_m, 10-08-00941-a, 11-02-01202-a, 11-07-00273-a, 11-08-00457-a).

REFERENCES

1. S. V. Zabotnov, L. A. Golovan', I. A. Ostapenko, Yu. V. Ryabchikov, A. V. Chervyakov, V. Yu. Timoshenko, P. K. Kashkarov, and V. V. Yakovlev, Pis'ma Zh. Eksp. Teor. Fiz. **83** (2), 76 (2006) [JETP Lett. **83** (2), 69 (2006)].
2. R. Wagner, J. Gottmann, A. Horn, and E. W. Kreutz, Appl. Surf. Sci. **252**, 8576 (2006).
3. A. Y. Vorobyev, V. S. Makin, and C. Guo, J. Appl. Phys. **101**, 034903 (2007).
4. Y. Yang, J. Yang, C. Liang, and H. Wang, Opt. Express **16**, 11259 (2008).
5. G. Miyaji and K. Miyazaki, Opt. Express **16**, 16265 (2008).
6. M. Huang, F. Zhao, Y. Cheng, N. Xu, and Z. Xu, Opt. Express **16**, 19354 (2008).
7. M. Huang, F. Zhao, Y. Cheng, N. Xu, and Z. Xu, Phys. Rev. B: Condens. Matter **79**, 125436 (2009).
8. S. Sakabe, M. Hashida, S. Tokita, S. Namba, and K. Okamuro, Phys. Rev. B: Condens. Matter **79**, 033409 (2009).
9. E. Stratakis, V. Zorba, M. Barberoglou, C. Fotakis, and G. A. Shafeev, Appl. Surf. Sci. **255**, 5346 (2009).
10. E. D. Diebold, N. H. Mack, S. K. Doorn, and E. Mazur, Langmuir **25**, 1790 (2009).
11. T. Baldacchini, J. E. Carey, M. Zhou, and E. Mazur, Langmuir **22**, 4917 (2006).
12. A. Y. Vorobyev and C. Guo, Appl. Phys. Lett. **94**, 224102 (2009); Opt. Express **18**, 6455 (2010).
13. J. E. Carey, C. H. Crouch, M. Shen, and E. Mazur, Opt. Lett. **30**, 1773 (2005).
14. A. Y. Vorobyev, V. S. Makin, and C. Guo, Phys. Rev. Lett. **102**, 234301 (2009).
15. A. V. Kabashin, M. Meunier, C. Kingston, and J. H. T. Luong, J. Phys. Chem. B **107**, 4527 (2003).
16. L. A. Golovan, I. O. Djun, A. E. Dokukina, S. V. Zabotnov, A. A. Ezhov, P. K. Kashkarov, N. E. Maslova, I. O. Ostapenko, V. I. Panov, and V. U. Timoshenko, Izv. Akad. Nauk, Ser. Fiz. **73** (1), 43 (2009) [Bull. Russ. Acad. Sci.: Phys. **73** (1), 39 (2009)].
17. R. Stoian, A. Mermillod-Blondin, N. M. Bulgakova, A. Rosenfeld, I. V. Hertel, M. Spyridaki, E. Koudoumas, P. Tzanetakis, and C. Fotakis, Appl. Phys. Lett. **87**, 124105 (2005).
18. E. V. Golosov, V. I. Emel'yanov, A. A. Ionin, Yu. R. Kolobov, S. I. Kudryashov, A. E. Ligachev, Yu. N. Novoselov, L. V. Seleznev, and D. V. Sinitsyn, Pis'ma Zh. Eksp. Teor. Fiz. **90** (2), 116 (2009) [JETP Lett. **90** (2), 107 (2009)].
19. J. E. Sipe, J. F. Young, J. S. Preston, and H. M. van Driel, Phys. Rev. B: Condens. Matter **27**, 1141 (1983).
20. S. A. Akhmanov, V. I. Emel'yanov, N. I. Koroteev, and V. N. Seminogov, Usp. Fiz. Nauk **147** (4), 675 (1985) [Sov. Phys.—Usp. **28** (12), 1084 (1985)].
21. A. Borowiec and H. K. Hagen, Appl. Phys. Lett. **82**, 4462 (2003).
22. N. Yasumaru, K. Miyazaki, and J. Kiuchi, Appl. Phys. A: Mater. Sci. Process. **76**, 983 (2003).
23. J. Bonse, M. Munz, and H. Sturm, J. Appl. Phys. **97**, 013538 (2005).
24. V. D. Zvorykin, A. A. Ionin, S. I. Kudryashov, Yu. N. Ponomarev, L. V. Seleznev, D. V. Sinitsyn, and B. A. Tikhomirov, Pis'ma Zh. Eksp. Teor. Fiz. **88** (1), 10 (2008) [JETP Lett. **88** (1), 8 (2008)].
25. A. Couairon and A. Mysyrowicz, Phys. Rep. **441**, 47 (2007).
26. S. M. Klimentov, T. V. Kononenko, P. A. Pivovarov, V. I. Konov, A. M. Prokhorov, D. Breitling, and F. Dausinger, Kvantovaya Elektron. (Moscow) **32**, 433 (2002).
27. M. Ye and C. P. Grigoropoulos, J. Appl. Phys. **89**, 5183 (2001).
28. *Handbook of Optical Constants of Solids*, Ed. by E. D. Palik (Academic, Orlando, Florida, United States, 1998).
29. A. Aguayo, G. Murrieta, and R. de Coss, Phys. Rev. B: Condens. Matter **65**, 092106 (2002).

30. R. H. M. Groeneveld, R. Sprik, and A. Lagendijk, Phys. Rev. B: Condens. Matter **51**, 11433 (1995).

31. S. I. Kudryashov and V. I. Emel'yanov, Pis'ma Zh. Eksp. Teor. Fiz. **73** (12), 751 (2001) [JETP Lett. **73** (12), 666 (2001)].

32. V. S. Makin, R. S. Makin, A. Ya. Vorobyev, and C. Guo, Pis'ma Zh. Tekh. Fiz. **34** (9), 55 (2008) [Tech. Phys. Lett. **34** (5), 387 (2008)].

33. V. P. Veiko, M. N. Libenson, G. G. Chervyakov, and E. B. Yakovlev, *Interaction of Radiation with Matter* (Fizmatlit, Moscow, 2008) [in Russian].

34. V. A. Soifer, Komp'yuternaya Opt. **32**, 110 (2008).

35. K. Ke, E. F. Hasselbrink, Jr., and A. J. Hunt, Anal. Chem. **77**, 5083 (2005).

36. I. S. Grigoriev and E. Z. Meilikhov, *Handbook of Physical Quantities* (Energoatomizdat, Moscow, 1991; CRC Press, Boca Raton, Florida, United States, 1997).

37. V. V. Klimov, *Nanoplasmonics* (Fizmatlit, Moscow, 2009; Pan Stanford, Singapore, 2011).

38. V. S. Makin, Fotonika, No. 2, 16 (2009).

Translated by M. Sapozhnikov